*Human Molecular Genetics, 2011, Vol. 20, No. 10* **2058–2070**
*doi:10.1093/hmg/ddr090*
*Advance Access published on March 9, 2011*

# Insufficiency of BUBR1, a mitotic spindle checkpoint regulator, causes impaired ciliogenesis in vertebrates

**Tatsuo Miyamoto[1], Sean Porazinski[2], Huijia Wang[2], Antonia Borovina[3,4], Brian Ciruna[3,4], Atsushi Shimizu[5], Tadashi Kajii[6], Akira Kikuchi[7], Makoto Furutani-Seiki[2] and Shinya Matsuura[1,*]**

[1]Department of Genetics and Cell Biology, Research Institute for Radiation Biology and Medicine, Hiroshima University, Hiroshima 734-8553, Japan, [2]Centre for Regenerative Medicine, Department of Biology and Biochemistry, University of Bath, Bath BA2 7AY, UK, [3]Program in Developmental & Stem Cell Biology, The Hospital for Sick Children, Toronto, Ontario, Canada M5G 1X8, [4]Department of Molecular Genetics, University of Toronto, Toronto, Ontario, Canada M5S 1A8, [5]Department of Molecular Biology, Keio University School of Medicine, 35 Shinanomachi, Shinjuku-ku, Tokyo 160-8582, Japan, [6]Hachioji, Tokyo 192-0023, Japan and [7]Department of Molecular Biology and Biochemistry, Graduate School of Medicine, Osaka University, Osaka 565-0870, Japan

Received November 25, 2010; Revised and Accepted February 28, 2011

**Budding uninhibited by benzimidazole-related 1 (BUBR1) is a central molecule of the spindle assembly checkpoint. Germline mutations in the budding uninhibited by benzimidazoles 1 homolog beta gene encoding BUBR1 cause premature chromatid separation (mosaic variegated aneuploidy) [PCS (MVA)] syndrome, which is characterized by constitutional aneuploidy and a high risk of childhood cancer. Patients with the syndrome often develop Dandy–Walker complex and polycystic kidneys; implying a critical role of BUBR1 in morphogenesis. However, little is known about the function of BUBR1 other than mitotic control. Here, we report that BUBR1 is essential for the primary cilium formation, and that the PCS (MVA) syndrome is thus a novel ciliopathy. Morpholino knockdown of *bubr1* in medaka fish also caused ciliary dysfunction characterized by defects in cerebellar development and perturbed left–right asymmetry of the embryo. Biochemical analyses demonstrated that BUBR1 is required for ubiquitin-mediated proteasomal degradation of cell division cycle protein 20 in the G0 phase and maintains anaphase-promoting complex/cyclosome-CDC20 homolog 1 activity that regulates the optimal level of dishevelled for ciliogenesis.**

## INTRODUCTION

Budding uninhibited by benzimidazole-related 1 (BUBR1) is a central component of the spindle assembly checkpoint and checkpoint signalling. It has been shown that in early M phase, BUBR1 binds to cell division cycle protein 20 (CDC20), a co-activator of the anaphase-promoting complex/cyclosome (APC/C), and inactivates the APC/$C^{CDC20}$ until all chromosomes have made proper attachments to the mitotic spindle (1,2). When all the kinetochores establish bipolar attachment, BUBR1 becomes a substrate of APC/$C^{CDC20}$ and is degraded through ubiquitin-mediated proteolysis (3). It was also reported that BUBR1 binds to CDC20 to inhibit APC/$C^{CDC20}$ activity in G2 phase prior to mitotic onset (4,5). Therefore, BUBR1 functions as a pseudo-substrate inhibitor of APC/$C^{CDC20}$ in G2 to early M phase to prevent unscheduled degradation of specific APC/$C^{CDC20}$ substrates.

APC/C activity is controlled during the cell cycle through the binding of CDC20 or another co-activator, CDC20 homolog 1 (CDH1). CDC20 is expressed during S, G2 and M phases, but only associates with the APC/C during the M phase when several core subunits of the APC/C are phosphorylated by cyclin-dependent kinase1 (CDK1)/cyclin B.

*To whom correspondence should be addressed. Tel: +81 822575809; Fax: +81 822567101; Email: shinya@hiroshima-u.ac.jp

The activated APC/$C^{CDC20}$ initiates the metaphase–anaphase transition through ubiquitin-mediated degradation of securin and cyclin B (6). In the anaphase, CDC20 is released from the APC/C since the core subunits of APC/C are dephosphorylated through the inhibition of CDK1/cyclin B activity, and APC/$C^{CDC20}$ is no longer active by the end of mitosis. In contrast to CDC20, CDH1 is phosphorylated by CDK1/cyclin B during the M phase, and the CDH1 phosphorylation prevents it from binding the core APC/C subunits. Therefore, APC/$C^{CDH1}$ is inactive in early M phase and becomes active from late M to G1 phases once APC/$C^{CDC20}$ has inhibited CDK1/cyclin B activity (6). The activated APC/$C^{CDH1}$ then targets several substrates, including CDC20 and CDH1 itself, to maintain the G1 and G0 phases.

Constitutional mutations in the budding uninhibited by benzimidazoles 1 homolog beta (BUB1B) gene encoding BUBR1 cause a rare human disorder—the premature chromatid separation syndrome [PCS (MIM 176430)], also known as the mosaic variegated aneuploidy (MVA) syndrome (MIM 257300). The PCS (MVA) syndrome is characterized by PCS in >50% metaphase cells, a variety of mosaic aneuploidies (gain or loss of whole chromosomes), severe intrauterine growth and mental retardation, and a high risk of childhood cancers (7,8). Both biallelic (7) and monoallelic (8) mutations of *BUB1B* have been found in individuals with the syndrome that resulted in low overall BUBR1 abundance. The clinical findings in the patients included the Dandy–Walker complex (9/16 patients), postcerebellar cyst (1/16), hypoplasia of the cerebellar vermis (1/16), lissencephaly (1/16), polycystic, often bilateral, nephroblastoma (7/16), polycystic kidney (2/16) and infantile obesity (2/11). These clinical features imply a critical role of BUBR1 in morphogenesis. However, little is known about the function of BUBR1 other than mitotic control. Using cell lines from the patients with the syndrome, we demonstrate that BUBR1 is essential for the formation of primary cilium; a microtubule-based organelle on the surface of most vertebrate cells in G0 phase, and that the PCS (MVA) syndrome is a novel ciliopathy. The primary cilium is regulated by APC/$C^{CDH1}$ activity through ubiquitin-mediated proteolysis of dishevelled (DVL) (9). Therefore, we studied the APC/C activity in G0 phase in the cells from the patients. We demonstrate that BUBR1 has a novel role for the maintenance of the APC/$C^{CDH1}$ activity in G0 phase that regulates the optimal level of DVL for ciliogenesis through proteasomal degradation of CDC20.

## RESULTS

### PCS (MVA) syndrome, a human condition of BUBR1 insufficiency, is a novel ciliopathy

Patients with the PCS (MVA) syndrome show Dandy–Walker complex, postcerebellar cyst, hypoplasia of the cerebellar vermis, lissencephaly, polycystic, often bilateral, nephroblastoma, polycystic kidney and infantile obesity (Fig. 1A). Since some of the clinical features were suggestive of impaired cilia formation (10–12), we speculated that the PCS (MVA) syndrome has ciliary dysfunction. Therefore, immortalized skin fibroblasts (PCS1 and MY1) from two unrelated patients with the PCS (MVA) syndrome were synchronized with serum starvation at G0 phase, and analysed for ciliogenesis (Fig. 1B and C). As much as 30% of cells from a normal individual (SM) were ciliated, but only 4% of MY1 cells and 1% of PCS1 cells were ciliated. PCS1 cells transferred with a whole chromosome 15 containing the *BUB1B* locus (hereafter called PCS1-Ch.15 cells) (8,13) showed restored ciliogenesis. Primary skin fibroblast cells from the two patients (PCS1sk and MY1sk) (8,13) also showed reduced ciliogenesis, as did Madin–Darby canine kidney (MDCK) cells transfected with a short-interfering RNA (siRNA) targeting *BUB1B* (Supplementary Material, Fig. S1A and C). These results indicate that cells with BUBR1 insufficiency have impaired ciliogenesis, and that the PCS (MVA) is a novel ciliopathy.

### Apical docking of basal body is impaired in the PCS (MVA) syndrome

In many cells in G0 phase, centrosomes migrate to the cell surface and are anchored to the membrane (apical docking), and primary cilia are assembled from the basal bodies (12). Immunostaining experiments revealed that in PCS1-Ch.15 cells BUBR1 is localized in the basal body, and that in PCS1 cells the signal for BUBR1 on the centrosome was dramatically reduced (14) (Fig. 1D). We then examined the apical docking of centrosomes under a confocal microscopy to learn how reduced levels of BUBR1 affect ciliogenesis. Centrosomes in cultured revertant PCS1-Ch.15 cells were localized to the apical surface, but those in PCS1 cells failed to dock apically and localized randomly (Fig. 2A–C). Transmission electron microscopy supported that the centrosomes in PCS1 cells failed to localize apically and remained in the cytoplasm (Fig. 2D). These results indicate that BUBR1 is required for apical docking of basal bodies.

### BUBR1 in G0 phase is required for APC/$C^{CDH1}$-mediated proteosomal degradation of DVL

Optimal levels of DVL, a core regulator protein in Wnt signalling, have been shown to be indispensable for apical docking of basal bodies, and both accumulation and attenuation of DVL lead to defective ciliogenesis (9,15,16). We, therefore, examined the levels of DVL1, DVL2 and DVL3 in PCS (MVA) syndrome cells. Since DVL2 is dominantly expressed in PCS1 cells as described below, DVL2 was compared with that of the revertant PCS1-Ch.15 cells. DVL2 was increased in both nuclear and cytoplasmic fractions (Fig. 3A). Primary skin fibroblast cells from these patients (PCS1sk and MY1sk) and *BUB1B* siRNA-transfected MDCK cells all showed increased DVL2 levels (Supplementary Material, Fig. S1B and D). Consistent with the high levels of DVL2, its downstream target, active β-catenin, was increased in a nuclear fraction and increased Wnt signalling was observed in PCS (MVA) syndrome cells (Fig. 3A and Supplementary Material, Fig. S2A–C). Next, we examined whether DVL2 or active β-catenin is involved in ciliary dysfunction in PCS1 cells. Induced expression of DVL2 in PCS1-Ch.15 cells suppressed ciliogenesis (Supplementary Material, Fig. S3C). In addition, knockdown of both DVL2 and DVL3 in PCS1 cells resulted in partial recovery of ciliogenesis (Fig. 4). On the other hand, treatment with Wnt/β-catenin signalling inhibitors, FH535 or

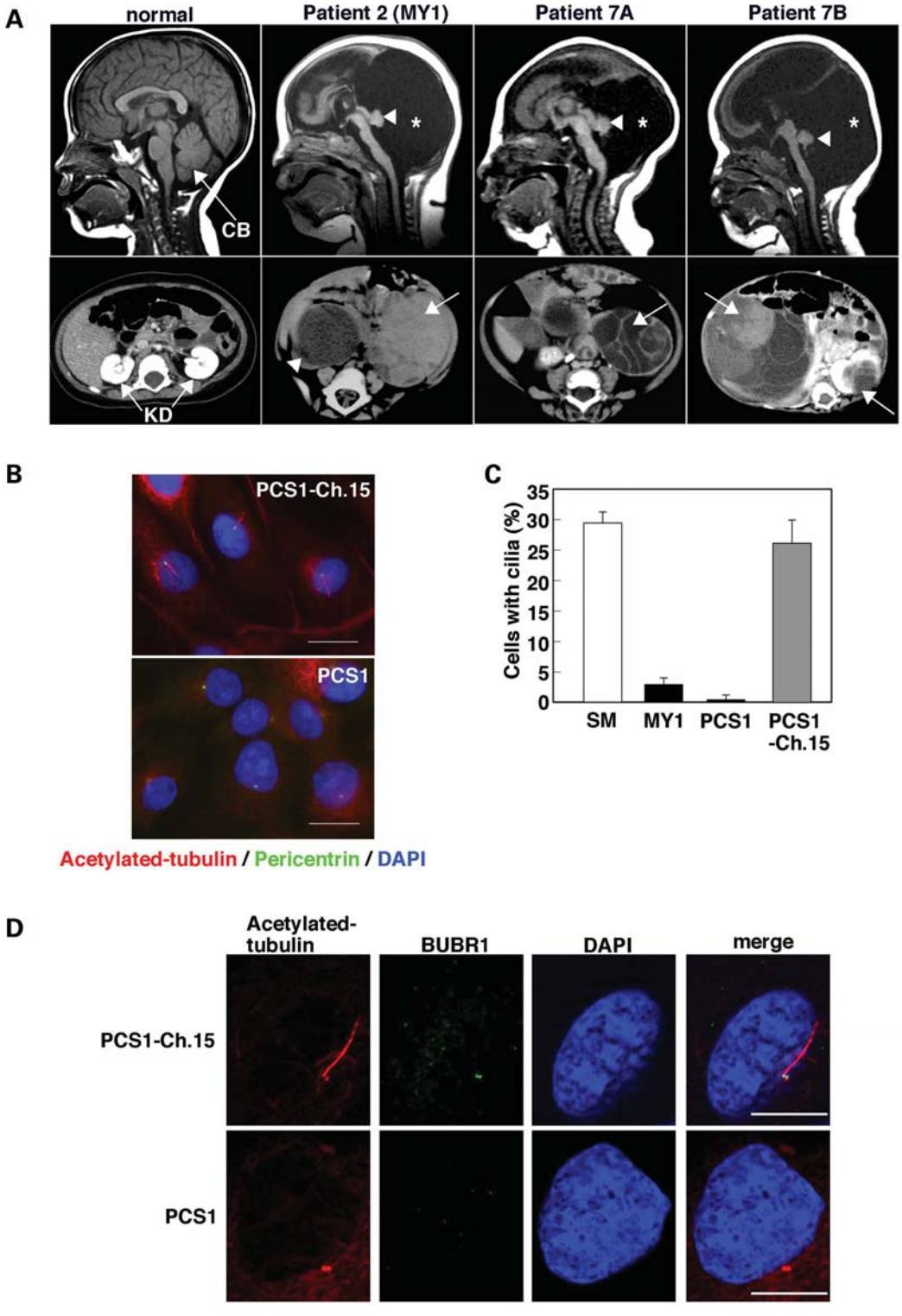


**Figure 1.** Human PCS (MVA) syndrome is a novel ciliopathy. (**A**) Normal individual. Patients 2, 7A, and 7B (8). MY1 cells used in this study were derived from patient 2 (8). Patients 7A and 7B are the siblings carrying a heterozygous single-base deletion 1833delT, the same mutation as the one found in patient 1 (PCS1), and a conserved haplotype around *BUB1B* that links to a modest decrease in their transcripts (8). Mid-sagittal views of head MRI showing Dandy–Walker complex with hypoplasia of the cerebellar vermis (arrowheads) and enlarged posterior fossae (asterisks). Abdominal CT images of multicystic nephroblastoma (arrows) and a cystic kidney (arrowhead). (**B** and **C**) Analysis of serum starvation-induced ciliogenesis in immortalized fibroblast cells from two patients (PCS1 and MY1) and a normal individual (SM). Both PCS1 and MY1 cells showed decreased ciliated cells. Microcell-mediated transfer of a human chromosome 15 (containing the *BUB1B* locus) restored the reduced ciliogenesis in PCS1 cells (PCS1-Ch.15 cells). Bar: 40 μm. (**D**) Immunofluorescence analyses of BUBR1 and acetylated tubulin in PCS1-Ch.15 cells and PCS1 cells in G0 phase. BUBR1 is localized to the basal body in PCS1-Ch.15 cell, whereas signal for BUBR1 on the basal body was severely reduced in PCS1 cells. Bar: 20 μm.

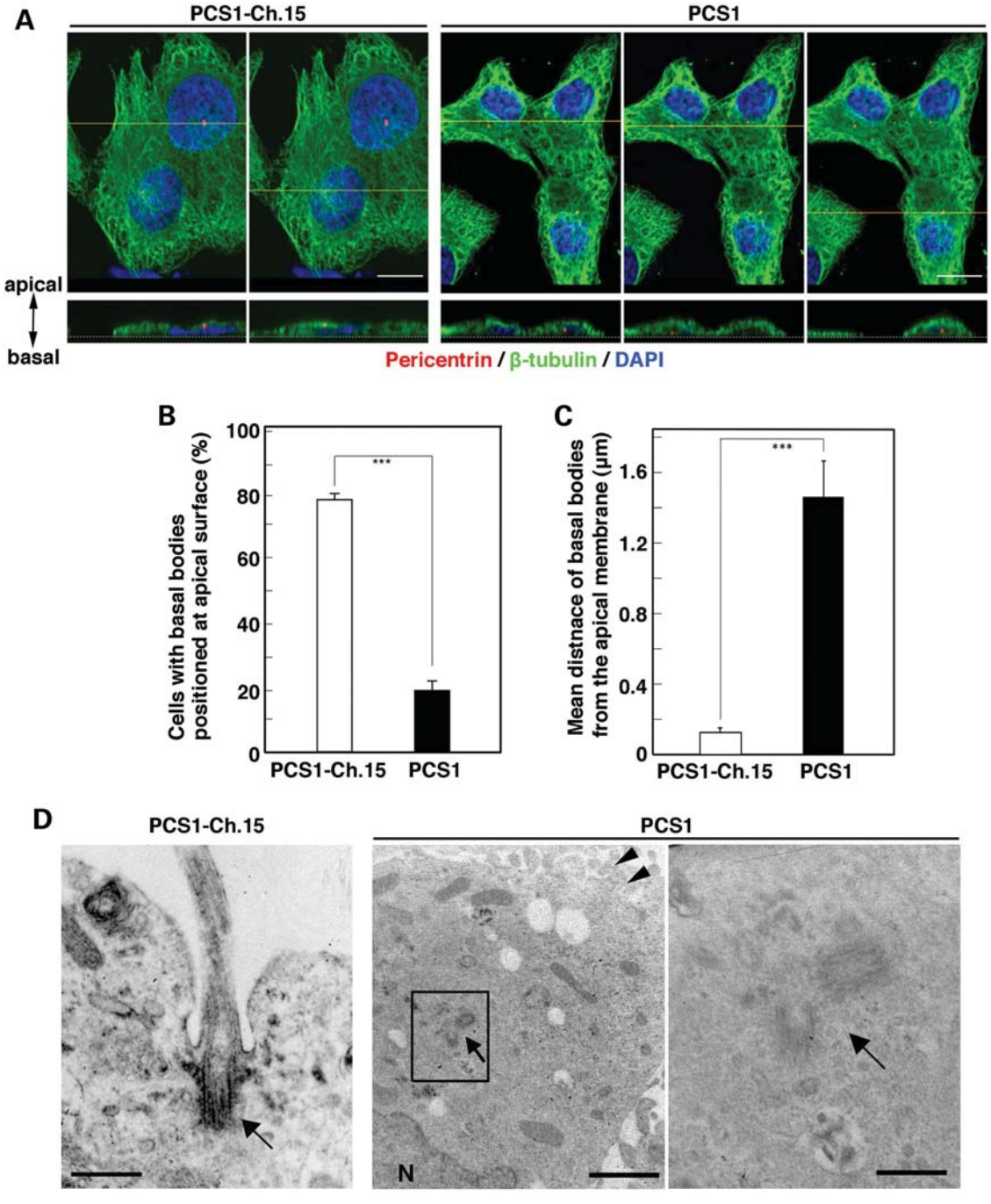


**Figure 2.** Basal bodies fail to dock at the apical membrane in the PCS (MVA) syndrome. (**A**) Surface view of a three-dimensional confocal microscopic image (upper panel), and cross-section view (lower panel) at an indicated yellow line showing basal bodies (red, Pericentrin), cellular β-tubulin network (green) and nuclei (blue, DAPI). A white-dotted line shows basal position of a cell. PCS1-Ch.15 cells showed localization of the basal bodies to the apical surface of the cells. In contrast, PCS1 cells show randomized localization of the basal bodies. Bar: 40 μm. (**B**) The differences in the apical position of basal bodies were statistically significant (***$P < 0.01$). For each cell line, >100 cells were scored. (**C**) The mean distance of basal bodies from the apical membrane in PCS1 cells was longer than that of PCS1-Ch.15 cells (***$P < 0.01$). For each cell line, 50 cells were examined. (**D**) Transverse sections of PCS1 cells observed with transmission electron microscopy. A PCS1-Ch.15 cell showed normal outgrowth of a ciliary axoneme from a basal body (arrow) docked at the apical membrane (left). In PCS1 cells, centrosomes (arrow) failed to localize apically and remained in the cytoplasm (middle and right). Arrowheads in the middle image show microvilli at the apical membrane. Close inspection of the square region in the middle panel indicated that the PCS1 cell has no typical structure of basal body (right). Bar: 500 nm (left and right image), 1.5 μm (middle image).

inhibitor of Wnt response-1 (IWR-1), in PCS1 cells did not restore ciliogenesis, although Wnt activity was suppressed to the level of PCS1-Ch.15 cells (Supplementary Material, Fig. S2D and E). These results indicate that an excess amount of DVL, but not β-catenin, is associated with the failure of ciliogenesis in PCS (MVA) syndrome cells.

To clarify whether the DVL2 synthesis is enhanced or the DVL2 degradation is decreased in PCS1 cells, the DVL2

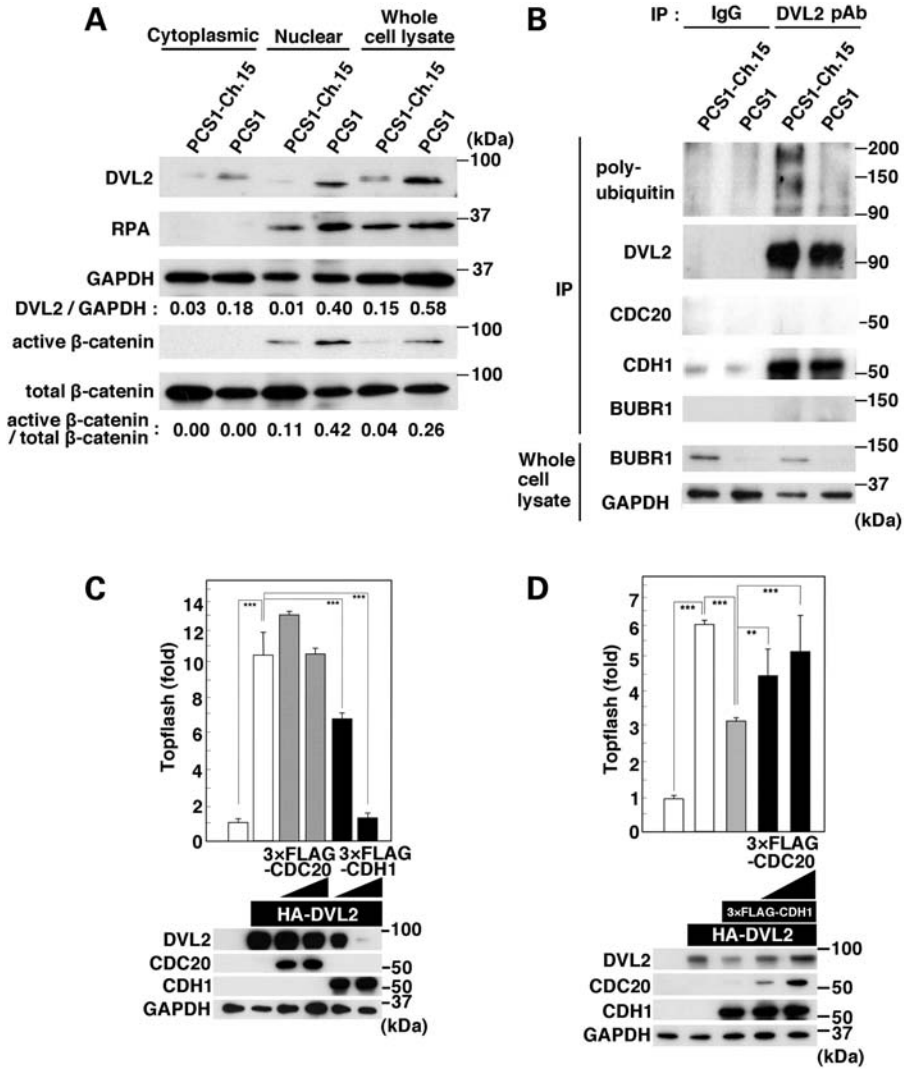


**Figure 3.** BUBR1 determines the stability of the DVL protein, an APC/$C^{CDH1}$ substrate, through its polyubiquitination. (**A**) Western blot analysis of Wnt signalling components in PCS1 cells. Whole cell lysates were separated to a cytoplasmic and a nuclear fraction. Replication protein A (RPA), a nuclear protein, served as a positive control for the nuclear fractionation. Dishevelled2 (DVL2) was increased in both a nuclear and cytoplasmic fraction from PCS1 cells. Active β-catenin (dephosphorylated form of β-catenin) was also increased in a nuclear fraction of PCS1 cells. The levels of DVL2 and active β-catenin were normalized to those of GAPDH and total β-catenin, respectively. (**B**) Immunoprecipitation and western blot analyses of DVL2 in PCS1 and PCS1-Ch.15 cells. Endogenous DVL2 was immunoprecipitated (IP) using an anti DVL2 polyclonal antibody and analysed for the ubiquitination state by western blotting with anti-FK1 monoclonal antibody. GAPDH served as a loading control. DVL2 was ubiquitinated in PCS1-Ch.15 cells, but the level of DVL2 ubiquitination was reduced in PCS1 cells. DVL2 interacted with CDH1, but not with CDC20 or BUBR1 in both PCS1 and PCS1-Ch.15 cells. These results suggest that APC/$C^{CDH1}$ but not APC/$C^{CDC20}$ mediates the ubiquitination of DVL2 in a BUBR1-dependent manner. (**C**) Serum-starved HEK293T cells were transfected with an hemagglutinin (HA)-DVL2 vector and a 3xFLAG-CDC20 (or CDH1) vector as indicated, and DVL2 levels were analysed by immunoblotting and Wnt signalling activity was analysed using a TCF/LEF-1-dependent luciferase reporter construct (Topflash). Transfection of the HA-DVL2 vector induced a high level of HA-DVL2 expression and Topflash activation. 3xFLAG-CDH1 expression, but not CDC20 expression, significantly suppressed HA-DVL2 expression and Topflash activation. (**D**) CDC20 inhibits APC/$C^{CDH1}$ activity in G0 phase. Serum-starved HEK293T cells were transfected with the HA-DVL2, 3xFLAG-CDH1 and 3xFLAG-CDC20 vector as indicated, and analysed. 3xFLAG-CDC20 expression dramatically induced HA-DVL2 expression and Topflash activation. The statistical significance of the difference was examined by *t*-test. $^{**}P < 0.05$ and $^{***}P < 0.01$.

protein was analysed by western blotting in serum-starved cells after treatment with the protein synthesis inhibitor cycloheximide (Chx) or proteasome inhibitor MG132. The level of DVL2 in PCS1-Ch.15 cells was substantially decreased after Chx treatment and increased after MG132 treatment (Supplementary Material, Fig. S3A). These results indicated that DVL2 is continuously synthesized and degraded in the cells. In contrast, Chx treatment did not decrease the DVL2 level in PCS1 cells, suggesting that the DVL2 synthesis is not increased in PCS1 cells. Additionally, MG132 did not increase the DVL2 level in PCS1 cells, suggesting that proteasome-dependent DVL2 degradation is defective in PCS1 cells. Therefore, we examined the ubiquitination state of DVL2 in PCS1 cells, PCS1-Ch.15 cells and cultured human embryonic

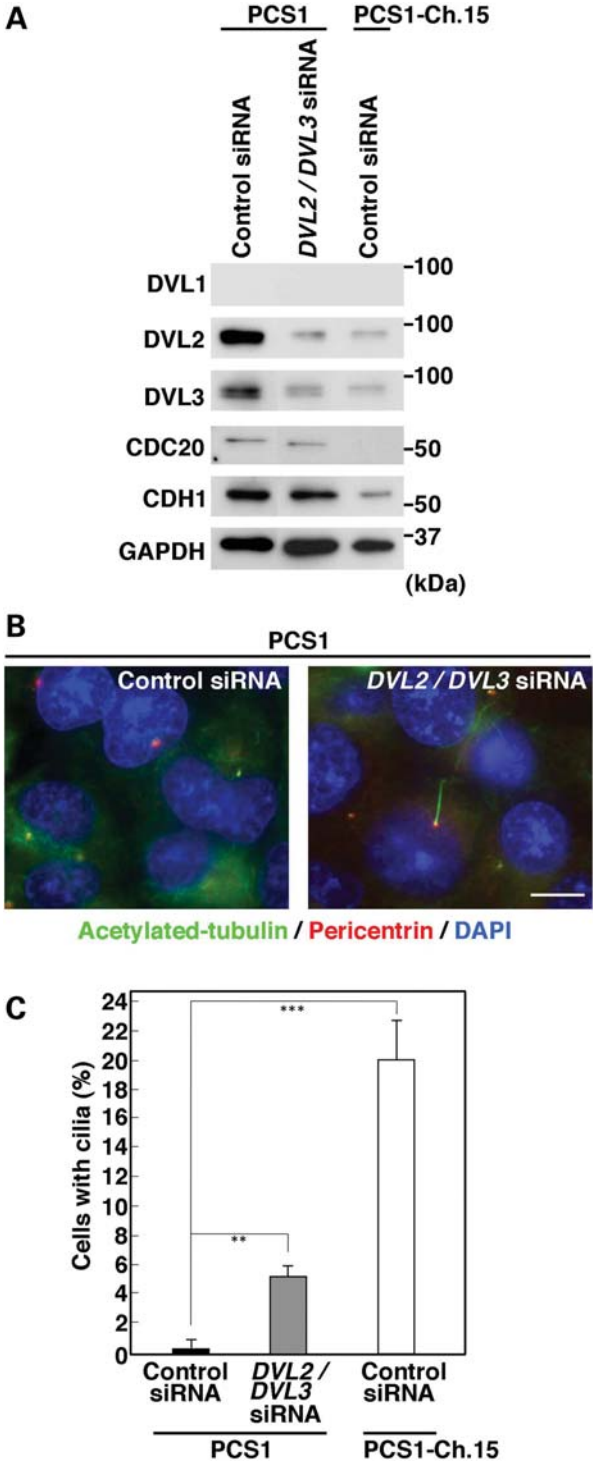


**Figure 4.** Knockdown of DVL partially restores ciliogenesis in PCS (MVA) syndrome cells. (**A**) Knockdown of *DVL2/DVL3* reduces the expression level of DVLs in PCS1 cells. Western blot analysis of DVLs, CDH1 and CDC20 in PCS1-Ch.15 cells and PCS1 cells after transfection of a siRNA targeting the conserved sequence between *DVL2* and *DVL3*. GAPDH served as a loading control. (**B**) Knockdown of DVL2/DVL3 rescued partially ciliogenesis in PCS1 cells. PCS1 cells transfected with control siRNA or *DVL2/DVL3* siRNA are shown. Primary cilia were stained with an anti-acetylated tubulin antibody (green), centrosomes were stained with an anti-Pericentrin antibody (red) and DNA was stained with DAPI (blue). Bar: 40 μm. (**C**) The differences in ciliogenesis were statistically significant ($^{**}P < 0.05$; $^{***}P < 0.01$).

kidney (HEK293T) cells. DVL2 was polyubiquitinated in PCS1-Ch.15 cells and normal HEK293T cells, while the ubiquitination level was decreased in PCS1 cells and *BUB1B* knockdowned HEK293T cells (Fig. 3B and Supplementary Material, Fig. S3B). DVLs contain a destruction box (D-box: RXXL) that is recognized by APC/C (9), and an L435S mutation in the D-box inhibited ubiquitination of DVL2 (Supplementary Material, Fig. S3B), suggesting that APC/C ubiquitinates DVL2 in normal cells. Since APC/C activity is controlled through the binding of two co-activators, CDC20 and CDH1 (2), we examined which co-activator is involved in the APC/C-mediated DVL2 proteolysis. Induced expression of CDH1 in HEK293T cells reduced the DVL2 level and suppressed Wnt signalling, while overexpression of CDC20 did not (Fig. 3C), indicating that CDH1, but not CDC20, promotes the APC/C-mediated DVL2 proteolysis. The reduction in the DVL2 level (and Wnt activity) by CDH1 was inhibited by a gradual increase in CDC20 (Fig. 3D), indicating that CDC20 antagonizes the APC/$C^{CDH1}$ activity. These results demonstrated that DVL is degraded through the APC/$C^{CDH1}$-mediated proteolysis in G0 phase, and BUBR1 is required for the APC/$C^{CDH1}$ activity.

### BUBR1 maintains APC/$C^{CDH1}$ activity for ciliogenesis through proteasomal degradation of CDC20

To address the mechanism for the regulation of APC/$C^{CDH1}$ activity by BUBR1, the expressions of CDC20 and CDH1 during the cell cycle were examined. In PCS1-Ch.15 cells, CDC20 was detected in S, G2 and M phases but not in G0 phase, as previously reported in normal cells (1,2). In contrast, in PCS1 cells, CDC20 was highly expressed in G0 phase (Fig. 5A). The proteasome inhibitor MG132 blocked the degradation of CDC20 (and DVL2) in serum-starved PCS1-Ch.15 cells, whereas PCS1 cells showed high levels of CDC20 (and DVL2) even in the absence of MG132 (Supplementary Material, Fig. S4A), suggesting that in G0 phase CDC20 is ubiquitinated in normal cells in a BUBR1-dependent manner. We, therefore, examined the ubiquitination state of CDC20 exogenously expressed in serum-starved normal (HEK293T) cells. CDC20 was polyubiquitinated in serum-starved HEK293T cells, and the ubiquitination level was decreased after BUBR1 depletion (Fig. 5B). CDC20 interacts with CDC27 (APC3), a core subunit of the APC/C, in a BUBR1-dependent manner (Supplementary Material, Fig. S4B). The region comprising residues 490–560 and the D-box motif in BUBR1 is, respectively, required for the binding with CDC20 and CDC27 (APC3) in serum-starved HEK293T cells (Supplementary Material, Fig. S5). These biochemical results suggest that BUBR1–APC/C complex mediates polyubiquitination of CDC20 in quiescent normal cells. As mentioned above, CDC20 antagonized the APC/$C^{CDH1}$ activity in G0 phase. Consistent with this, knockdown of CDC20 in PCS1 cells resulted in a reduction in DVL2 (Fig. 5C) and partial recovery of ciliogenesis (Fig. 5D and E). These results indicate that a high amount of CDC20 in PCS1 cells impairs the APC/$C^{CDH1}$-mediated DVL2 ubiquitination for ciliogenesis. PCS1 cells also showed high levels of CDH1 in G0 phase (Fig. 5A). Although BUBR1 in G0 phase did not bind to CDH1 directly, the interaction of CDH1 with

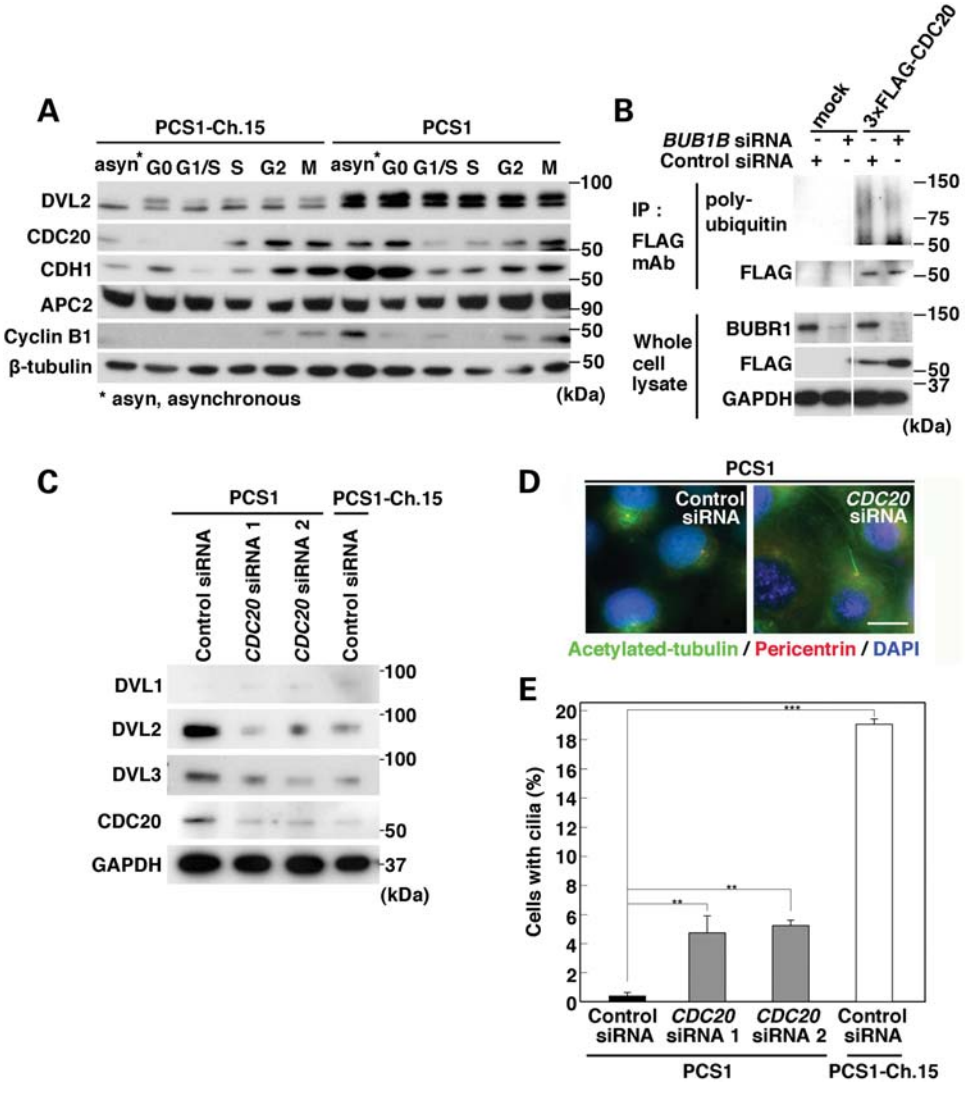


**Figure 5.** BUBR1-dependent CDC20 proteasomal degradation in G0 phase is required for ciliogenesis. (**A**) Levels of APC/C components during the cell cycle were analysed by western blotting. High levels of CDC20 and CDH1 were observed in PCS1 cells in the G0 phase. (**B**) BUBR1 is required for CDC20 ubiquitination in G0 phase. 3xFLAG-CDC20 and *BUB1B* siRNA (or control siRNA) were co-transfected into HEK293T cells. After serum starvation for 24 h, whole cell lysates were immunoprecipitated (IP) with anti-FLAG antibody, and the polyubiquitination state of CDC20 was evaluated by immunoblotting with anti-FK1 monoclonal antibody. *BUB1B* knockdown reduces the level of CDC20 ubiquitination. APC/$C^{CDH1}$, not APC/$C^{CDC20}$, is responsible for ubiquitin-mediated degradation of DVL2 in G0 phase. (**C**) Knockdown of *CDC20* reduces the expression level of DVL2 in PCS1 cells. Western blot analysis of DVLs in PCS1 cells after transfection of *CDC20* siRNA and PCS1-Ch.15 cells. GAPDH served as a loading control. The expression levels of DVL2 were decreased after transfection of *CDC20* siRNA. (**D**) Knockdown of CDC20 partially restored ciliogenesis in PCS1 cells. PCS1 cells transfected with control siRNA or *CDC20* siRNA are shown. Primary cilia were stained with an anti-acetylated tubulin antibody (green), centrosomes were stained with an anti-Pericentrin antibody (red) and DNA was stained with DAPI (blue). Bar: 40 μm. (**E**) The differences in ciliogenesis were statistically significant ($^{**}P < 0.05$; $^{***}P < 0.01$).

APC/C was impaired significantly after BUBR1 depletion in HEK293T cells (Supplementary Material, Fig. S4B). Since CDH1 is autonomously degraded by APC/$C^{CDH1}$ during G0 phase (17), the high levels of CDH1 might be the consequence of the decreased APC/$C^{CDH1}$ activity in PCS1 cells. Based on these results, we propose a model that in G0 phase BUBR1 binds to CDC20 (Supplementary Material, Fig. S4B) (18) to inhibit APC/$C^{CDC20}$ and instead activates APC/$C^{CDH1}$, thereby allowing DVL proteasomal degradation to establish its optimal level for ciliogenesis (Fig. 6).

## Medaka *bubr1* insufficiency causes ciliary dysfunction characterized by defects in cerebellum formation and perturbed left–right axis

To learn whether the functional role of BUBR1 for ciliogenesis is conserved in vertebrates, we induced BUBR1 insufficiency in medaka fish (*Oryzias latipes*) (19). *bubr1* (medaka homolog of *BUB1B*) expression is ubiquitous under normal conditions (Fig. 7A). Knockdown of *bubr1* with two distinct antisense morpholino oligonucleotides (knockdown efficacy

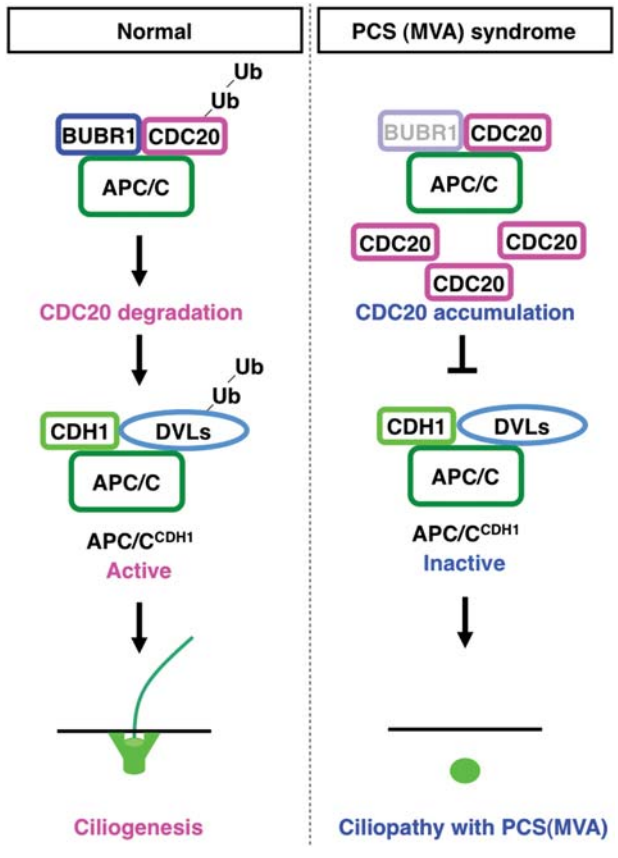


**Figure 6.** A model of the molecular function of BUBR1 in ciliogenesis. BUBR1-dependent CDC20 degradation in G0 phase cells plays a role in the maintenance of APC/$C^{CDH1}$ activity during primary cilia formation. In PCS (MVA) syndrome cells, insufficiency of BUBR1 results in CDC20 accumulation to inhibit APC/$C^{CDH1}$ activity in G0 phase. Excess amounts of DVLs, the targets of APC/$C^{CDH1}$, interfere apical docking of centrosomes to cause impaired ciliogenesis.

and specificity are shown in Fig. 7D and Supplementary Material, Figs. 6 and 7) perturbed the formation of the cerebellum (Fig. 7B), as observed in patients with the PCS (MVA) syndrome. *bubr1* morphants also showed perturbed left–right asymmetry of visceral organs including the liver, spleen, gut and cardiac looping (Fig. 7C and D and Supplementary Material, Fig. S7), although no patients with the syndrome with perturbed left–right asymmetry have been reported. Randomized expression of left–right asymmetry genes was observed, including the nodal ligand *southpaw* (*spaw*) and its downstream genes *lefty* and *pitx2* in the lateral plate mesoderm, which comprise the readout of cilium-generated fluid flow in Kupffer's vesicle, a teleost-specific organ equivalent to a mouse node (Supplementary Material, Fig. S8). The number of cilia in Kupffer's vesicle was significantly reduced (Fig. 7E and F), resulting in defective fluid flow (Fig. 7E and G and Supplementary Material, Movies S1 and S2). These results demonstrate a conserved role of BUBR1 for the primary cilium formation, but also suggest phenotypic heterogeneity between human and medaka fish.

## DISCUSSION

In mammalian cells, failure of spindle microtubule–kinetochore attachments in M phase activates BUBR1 to bind to CDC20 and inhibit APC/$C^{CDC20}$, leading to inhibition of chromosome separation (1,2,18,20). Although the inhibition of CDC20 by BUBR1 for spindle assembly checkpoint in M phase has been well established (1–5), the role of BUBR1 in G0 phase was unclear. We found that BUBR1 binds to CDC20 and the core APC/C subunits and forms a complex in G0 phase, and that siRNA-knockdown of BUBR1 in HEK293T cells impairs poly-ubiquitination of CDC20. These results demonstrate that in G0 phase BUBR1 inhibits APC/$C^{CDC20}$ activity through the proteasomal degradation of CDC20. Accumulation of CDC20 was observed in the PCS (MVA) syndrome cells, but was not likely to be the mitotic leakage, because in late M phase active APC/$C^{CDC20}$ causes its own inhibition and switches to APC/$C^{CDH1}$ activity independently of spindle assembly checkpoint (21). It was recently reported that BUBR1 binds to CDC20 to inhibit APC/$C^{CDC20}$ in interphase, thereby allowing accumulation of cyclin B in G2 phase prior to mitotic onset (4,5). Thus, BUBR1 may function as an inhibitor of APC/$C^{CDC20}$ not only in early M phase but also in multiple phases of the cell cycle.

Conditional knockdown of *APC2*, a core subunit of APC/C, in G0-quiescent hepatocytes in mice caused dedifferentiation and unscheduled proliferation of these cells, which may be attributed to the lack of APC/$C^{CDH1}$ activity (22). APC/$C^{CDH1}$ activity regulates axonal growth in postmitotic neurons (23). In the context of cilia formation, APC/$C^{CDH1}$ activity is indispensable for apical docking of basal body through the quantitative regulation of DVL by APC/$C^{CDH1}$ in *Xenopus* embryos (9). CDC14 phosphatases in vertebrates, *CDC14A* and *CDC14B*, both counteract CDH1 phosphorylation to activate APC/$C^{CDH1}$ activity during late M phase (24). Loss of *CDC14B* in zebrafish embryos caused ciliary dysfunction characterized by hydrocephaly, kidney cysts and left–right asymmetry defects (25). These findings suggested that APC/$C^{CDH1}$ activity in G0 phase is essential for cell differentiation and cell morphology (26). In spite of the functional significance of APC/$C^{CDH1}$, the maintenance mechanism in G0 phase was unclear. We showed that the accumulation of CDC20 in G0 phase interferes with the APC/$C^{CDH1}$-mediated proteolysis of DVL for ciliogenesis, and that BUBR1 is required for the maintenance of the APC/$C^{CDH1}$ activity in G0 phase.

The 'APC/$C^{CDH1}$–DVL proteolysis' axis in G0 phase is fundamental for ciliogenesis. Our data demonstrated that BUBR1 in G0 phase maintains the APC/$C^{CDH1}$ activity to establish the 'BUBR1–APC/$C^{CDH1}$–DVL proteolysis' axis for ciliogenesis. It was reported that inversin (NPHP2), an underlying protein for the ciliopathy in both human and mouse, binds to DVL and promotes the ubiquitination of DVL by APC/$C^{CDH1}$ (15). Loss of *inversin* leads to increased amounts of DVL and ciliary dysfunction similarly to the PCS (MVA) syndrome. Therefore, the PCS (MVA) syndrome and inversin-mutated ciliopathy (nephronophthisis) may have a common pathological pathway, and BUBR1 may act epistatically upstream of both inversin and DVL to maintain APC/$C^{CDH1}$ activity for ciliogenesis, because inversin is also a direct substrate of APC/$C^{CDH1}$ (15).

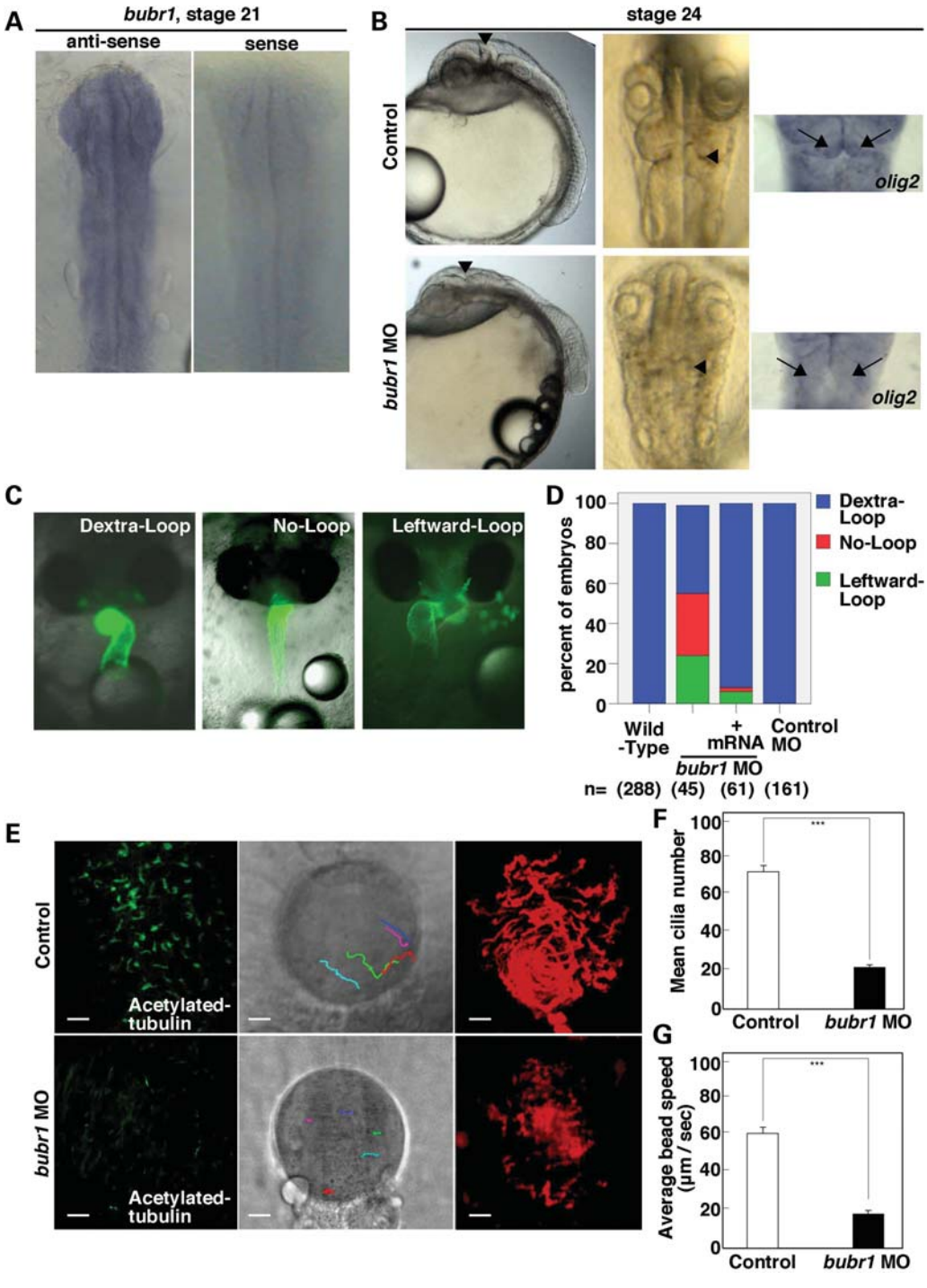


**Figure 7.** Morpholino knockdown of *bubr1* in medaka fish causes ciliary dysfunction. (**A**) Left panel shows ubiquitous expression of *bubr1* at stage 21 (six somites). Right panel is a negative control for *in situ* hybridization of *bubr1*. (**B**) Phenotypes of medaka *bubr1* morphants (MO). Lateral views of whole body and dorsal views of head formation at stage 24 (16 somites). *bubr1* morphants (6 of 26 injected embryos) exhibit reduction of the mid-hindbrain (arrowheads). Cerebellum (arrows) detected by *olig2* expression. *bubr1* morphants (22/28) show defective cerebellar development. (**C**) Heart laterality defects in *bubr1* morphants. Randomized heart looping in *bubr1* morphants was partially rescued in *bubr1* mRNA co-injected embryos. Images of normal heart looping (Dextra-Loop), no heart looping and reversed heart looping (Leftward-Loop) in frontal views of *cmcl2*-enhanced green fluorescent protein (EGFP)-labelled hearts at stage 28 (30 somites). (**D**) A graph showing the proportion of *bubr1* morphants displaying laterality defects in the heart. (**E**–**G**) Ciliary defects in Kupffer's vesicle (KV) of a *bubr1* morphant. Confocal images of embryos at stage 21 showing the KV labelled with an anti-acetylated-tubulin antibody (bars: 80 μm), and the statistics of the number.*bubr1* morphants ($n = 5$) have fewer cilia than controls ($n = 7$) (F). The statistical significance of the differences was examined by *t*-tests. $^{***}P < 0.01$. Bright-field and Z-stack projections (red) of fluorescent time-lapse images of KVs injected with fluorescent beads at stage 21(bars: 10 μm) are shown in the middle and right panels, respectively (E). Coloured lines in middle panel indicate representative bead trajectories. In wild-type KVs, a general counter-clockwise flow is observed ($n = 7$; see Supplementary Material, Movie S1). In morphants, only random Brownian motion is observed ($n = 7$; see Supplementary Material, Movie S2) (bars: 10 μm). The bead speeds are much slower in *bubr1* morphants than in control morpholino-injected embryos (G).

Ciliogenesis is regulated dynamically in a cell cycle-dependent manner (27). While ciliogenesis occurs in G0/G1 phase, cilia disassembly begins when G0-quiescent cells re-enter the cell cycle and become irreversibly committed to DNA replication in late G1 phase (27,28). We showed that BUBR1, a cell cycle regulator, plays a crucial role in cilia formation through the quantitative regulation of ciliary protein. It was also reported that some ciliary molecules control cell division program. In *Chlamydomonas*, IFT27, a Rab-like small G protein, is required for both cell proliferation and flagellum formation (29). A complex of two centrosomal proteins, CP110 and CEP92, promotes cell cycle progression and cilia disassembly in mammalian cells (30). Polycystin-1, -2 and polaris mediate chromosome segregation through the proper expression of survivin, a chromosome passenger protein (31). Thus, cross talk between cell cycle regulators and ciliogenesis machineries is essential for the cell cycle-dependent ciliary dynamics.

Both monoallelic and biallelic mutations of *BUB1B* have been found in individuals with the PCS (MVA) syndrome (7,8). Patients with monoallelic mutations were severely affected with the Dandy–Walker complex (9/11 patients), polycystic nephroblastoma (7/11) and rhabdomyosarcoma (5/11). On the other hand, patients with biallelic mutations showed a moderate phenotype: Dandy–Walker complex (0/5 patients), polycystic nephroblastoma (0/5) and rhabdomyosarcoma (2/5). These results suggest a possible correlation of *BUB1B* mutations with ciliopathy and cancer phenotypes.

In summary, our data demonstrate that BUBR1 is required for the maintenance of APC/$C^{CDH1}$ activity in G0 phase, and that failure of the maintenance of APC/$C^{CDH1}$ activity is responsible for the impaired ciliogenesis of the PCS (MVA) syndrome.

## MATERIALS AND METHODS

### Cell culture

The immortalized fibroblast cell lines from two patients with the PCS (MVA) syndrome (PCS1 and MY1), a fibroblast cell line from a normal individual (SM) and a chromosome 15-transferred PCS1 cells (PCS1-Ch.15) were described previously (8,13,14). In brief, the MY1 cell line was derived from patient 2 with a heterozygous intronic mutation IVS10-5A > G in *BUB1B*, which results in an aberrant splicing leading to a premature stop codon (W468fsX480) (8). The PCS1 cell line was established from patient 1 with a heterozygous single-base deletion 1833delT, which results in protein truncation (F611fsX625) (8). Although no mutation was found in the second alleles of the two patients, a conserved haplotype around *BUB1B* that links to a modest decrease of their transcripts was observed (8). All cell cultures were maintained in Dulbecco's modified eagle medium (DMEM) supplemented with 10% fetal bovine serum (FBS) at 37°C under 5% $CO_2$. Transfection of plasmids or siRNAs into cells was performed using the Lipofectamine 2000 reagent (Invitrogen) according to the manufacturer's protocol. At 24 h after transfection, the medium was replaced with serum-free DMEM, and the cells were incubated for 24 h to become Ki-67-negative and achieve quiescent G0 phase.

### Antibodies

The primary antibodies used were: mouse anti-acetylated tubulin monoclonal antibody (mAb) (Sigma); rabbit anti-Pericentrin polyclonal antibody (pAb) (Bethyl Laboratories); rat anti-β-tubulin mAb (Novus); mouse anti-β-tubulin mAb (Sigma); mouse anti-active β-catenin (clone 8E7) mAb (Millipore); mouse anti-β-catenin mAb (BD Transduction Laboratories); mouse anti-GAPDH mAb (Santa Cruz Biotechnology); mouse anti-RPA mAb (BD Transduction Laboratories); mouse anti-DVL1 mAb (Santa Cruz Biotechnology); rabbit anti-DVL2 mAb (Cell Signaling Technology Inc.); rabbit anti-DVL3 mAb (Cell Signaling Technology Inc.); rabbit anti-CDC20 pAb (Santa Cruz Biotechnology); mouse anti-CDH1 mAb (Thermo); mouse anti-APC2 mAb (Thermo); mouse anti-CDC27 mAb (BD Transduction Laboratories); mouse anti-Cyclin B1 mAb (BD Transduction Laboratories); mouse anti-polyubiquitinated proteins (clone FK1) mAb (Biomol); rabbit anti-GFP pAb (MBL); mouse anti-GFP mAb (Roche); mouse anti-DYKDDDDK (FLAG) tag mAb (Wako) and rabbit anti-hemagglutinin (HA) pAb (Santa Cruz Biotechnology). The rabbit anti-human BUBR1 pAb was raised and characterized previously (8,14).

### Plasmids

HA-tagged mouse DVL2 and enhanced green fluorescent protein (EGFP)-tagged human BUBR1 were described previously (14,32). We constructed a FLAG-tagged mouse DVL2 plasmid by polymerase chain reaction (PCR) and standard cloning techniques. We used site-directed mutagenesis to insert mutations into DVL2 and BUBR1. The mutations were verified by automated sequencing.

### Electron microscopy

Cells cultured on polycarbonate filters (Corning) were fixed with 4% paraformaldehyde and 2% glutaraldehyde in 0.1 M cacodylated buffer (pH 7.4) for 10 min at 37°C and then washed with 0.1 M phosphate buffer. Samples were post-fixed in 2% $OsO_4$ in the same buffer for 90 min on ice, dehydrated in ethanol and embedded in Epon 812. Thin sections were cut, double-stained with uranyl acetate and lead citrate for 4 min at room temperature and examined under an electron microscope (JEM-1200EX; Jeol) at an accelerating voltage of 80 kV.

### RNA interference

The following stealth siRNAs synthesized by Invitrogen were used: human *BUB1B*-1 (5′-UCAAGGGUUCAAUUCCUUCCUGUAAAUUC-3′); human *BUB1B*-2 (5′-AUACCAAACAGGUCUACCUGGUAGG-3′); dog *BUB1B*-1 (5′-UGGAGAUACAUCCUCAUUGGAGUUG-3′); dog *BUB1B*-2 (5′-AUCACUGGCAUUCAGAAUCCGCACA-3′); human *CDC20*-1 (5′-UUUGAGUUCAGCCACCUUGGCCAUG-3′) and human *CDC20*-2 (5′-AUUACCACCACUGGCCAAAUGUCGU-3′). Human *DVL2/DVL3* siRNA (5′-GUCAACAAGAUCACCUUCUTT-3′) synthesized by QIAGEN was used.

Stealth-negative control duplexes (Cat. No. 12935-300 and 12935-112; Invitrogen) were also used.

### Immunoprecipitation and western blot analyses

Cells were transfected with siRNAs or plasmid DNA, and cultured in serum-free DMEM for 24 h. The cells were lysed in lysis buffer (0.5% Triton X-100, 150 mM NaCl, 20 mM Tris–HCl pH 7.5, 1 mM ethylene-diamine-tetraacetic acid (EDTA), 0.5 mM phenyl-methyl-sulfonyl fluoride (PMSF), 2 mg/ml pepstatin A, 10 mg/ml leupeptin, 5 mg/ml aprotinin). The lysates were sheared with a 21-gauge needle, incubated on ice for 30 min and clarified by centrifugation at 20,817*g* for 15 min at 4°C. The supernatants were pre-cleared with protein A/G-conjugated agarose and incubated with anti-FLAG, anti-DVL2 or anti-GFP antibodies for 2 h at 4°C with constant rotation. Protein A/G-conjugated agarose was then added to the lysates and the mixtures were rotated for a further 12 h at 4°C. The agarose beads were washed three times with wash buffer (1% Nonidet P-40, 0.1% SDS, 0.5% deoxycholate, 150 mM NaCl, 50 mM Tris–HCl pH 7.5, 1 mM EDTA, 0.5 mM PMSF, 2 mg/ml pepstatin A, 10 mg/ml leupeptin, 5 mg/ml aprotinin) before elution with sample buffer. The immunoprecipitated proteins were analysed by 10% sodium dodecyl sulfate-polyacrylamide gel electrophoresis (SDS-PAGE) and transferred to polyvinylidene fluoride membranes for immunoblotting analyses.

### Immunofluorescence microscopy

Cells grown on cover slips were fixed in 100% methanol at −20°C for 10 min, briefly washed with phosphate buffered saline (PBS) three times, blocked with 1% bovine serum albumin (BSA) in PBS for 30 min and probed with primary antibodies. Antibody–antigen complexes were detected with Alexa Fluor 594- or Alexa Fluor 488-conjugated goat secondary antibodies (Molecular Probes) by incubation for 30 min at room temperature. The cells were washed three times with PBS and then counterstained with 4′,6′-diamidino-2-phenylindole (DAPI). Immunostained cells were examined under a fluorescence microscope (Zeiss Axioskop2; Carl Zeiss Microimaging Inc.) and a confocal microscope (FV1000-D; Olympus Inc.).

### Protein half-life assay

Cells were treated with 25 mg/ml Chx for 0, 2 or 4 h to determine the half-life of DVL2. To inhibit proteasome-dependent degradation, cells were treated with 5 mM MG132 (Sigma) for 5 h before harvesting.

### Cell fractionation

Cytoplasmic and nuclear extracts were prepared using a CelLytic NuCLEAR Extraction Kit (Sigma) according to the manufacturer's protocol.

### Cell-cycle synchronization

Cells were synchronized at the G1/S phase boundary by double-thymidine block, and at the G0 phase by serum starvation. For thymidine block, cells were incubated with 2 mM thymidine for 16 h, washed extensively with DMEM supplemented with 10% FBS, released for 8 h and subjected to a second thymidine block for 18 h and released.

### Luciferase assay

Cells ($1 \times 10^5$) were plated in 12-well plates. On the following day, the cells were transfected with 200 ng of Topflash or Fopflash luciferase reporter plasmid (Upstate Biotechnology) plus 2 ng of internal control plasmid pRL-TK (Promega) using the Lipofectamine 2000 reagent (Invitrogen). The transfected cells were lysed and analysed for their relative β-catenin/Tcf activities using a Dual-Luciferase Reporter Assay System (Promega). To inhibit Wnt/β-catenin signalling, 10 μM FH535 (Sigma) or 40 μM IWR-1 (Sigma) were added to the media at 24 h before luciferase assay.

### Medaka fish maintenance

Embryos of the Kyoto-Cab inbred medaka strain were used for all experiments (19). To visualize left–right asymmetry of the heart, the *cmcl2*-EGFP transgenic medaka line was used. Microinjection, raising and staging were carried out as previously described (33).

### Morpholino oligonucleotides and mRNA injections

The following morpholinos against two distinct domains of medaka *bubr1* pre-mRNA synthesized by Gene Tools LLC were used: translation-blocking morpholino (TBMO), 5′-ATTCCACATCACCACCTTCCGCCAT-3′; and splice-blocking morpholino (SBMO), 5′-TATATCTGTAAGGAGTCAACCAGGT-3′. For negative controls, a standard control morpholino (5′-CCTCTTACCTCAGTTACAATTTATA-3′) was used. A volume of 1 nl was injected with 5 ng of SBMO, 1.5 ng of TBMO or an equivalent amount of control morpholinos to each *bubr1* morphant.

Capped medaka *bubr1* mRNA was synthesized using an mMessage Machine SP6 Transcription Kit (Ambion) from the full-length medaka *bubr1* cDNA in pCS2+ cloned by RT–PCR. For rescue experiments, 100 pg of *bubr1* mRNA was coinjected with 1.5 ng of *bubr1* TBMO into one-cell-stage embryos.

### RT–PCR

Total RNA was extracted from 10 each of wild-type or SBMO (5 ng)-injected embryo pools using the TRIzol reagent (Invitrogen) according to the manufacturer's protocol. First-strand cDNAs were generated with an oligo (dT) primer using an RNA PCR™ Kit (AMV) Ver. 3.0 (Takara Bio Inc.). To examine the efficacy of the SBMO targeted toward the intron–exon boundary of exon 4, primers spanning exon 3 (5′-AGACGATCCTCTTGGTGTT-3′) and exon 5 (5′-TTTGCGAAAGTTGCCCTG-3′) were designed. PCR amplification was performed with TaKaRa Ex Taq HS (Takara Bio Inc.) using the cDNAs from the wild-type and morpholino-injected embryos in three independent experiments.

### *In situ* hybridization

Whole-mount *in situ* hybridization analyses were carried out as described previously (33). Digoxigenin-labelled RNA probes were generated using a DIG RNA Labeling Kit (Roche). cDNA templates for *bubr1*, *spaw*, *lefty*, *pitx2* and *olig2* were cloned into pBluescript SK- by RT–PCR.

### Analysis of Kupffer's vesicle (KV) flow

Dechorionated embryos were mounted in 1.5% low-melting agarose. Fluorescent beads (1.0 μm; Invitrogen) were injected into KVs and imaged using an MZ16FA microscope (Leica) with a DFC350FX digital camera. The bead trajectories were traced by sequential time-lapse images using ImageJ 1.42q software (NIH).

### Imaging of cilia in KVs

Ciliogenesis in medaka embyos was analysed by both immunohistochemistry and live imaging. Whole-mount antibody staining was performed as previously described (33). The antibodies used were an anti-acetylated α-tubulin antibody (1:200; Sigma T-6793) and an Alexa Fluor 488-conjugated anti-mouse IgG secondary antibody (1:500; Invitrogen). For live imaging of cilia, mARL13b-GFP mRNA (34) was injected into 1-cell-stage embryos and dechorionated embryos at stage 21 (34 hpf) were used. Immunostained or mRNA-injected embryos were mounted in agarose and imaged using an SP2 confocal microscope (Leica).

The number of cilia was quantified by counting every cilium in the tissue of interest using ImageJ 1.42q software (NIH). SPSS software ver. 16.0 (SPSS Inc.) was used to carry out two-sample *t*-tests to compare the cilia numbers in tissues of interest in TBMO-injected embryos with those in uninjected wild-type embryos. Values of $P < 0.01$ were considered to be statistically significant.

### Statistical analysis

The experiments were performed at least three times, and the data are shown as means ± standard error of the mean. Statistical analyses were performed using StatView software (SAS Institute). Differences between the data were tested for statistical significance using Student's *t*-test. Values of $P < 0.05$ were considered to be statistically significant.

## SUPPLEMENTARY MATERIAL

Supplementary Material is available at *HMG* online.

## ACKNOWLEDGEMENTS

We thank M. Kobayashi, T. Takumi and S. Horita for providing clinical information, and C. Tickle, F. Bangs, S. Bagby and L. Hurst (University of Bath) for valuable comments and critical reading of the manuscript. We also thank Y. Tonouchi for technical support and K. Koike (Center for Gene Science, Hiroshima University) for electron microscopy observations.

*Conflict of Interest statement*. None declared.

## FUNDING

This work was supported by a Grant-in-Aid for Scientific Research (to S.M.) and a Grant-in-Aid for Cancer Research (to S.M. and T.M.) from the Ministry of Education, Culture, Sports, Science and Technology of Japan, a Hiroshima University Support Foundation grant (to T.M.) and a Hiroshima University Fujii Memorial Foundation grant (to T.M.). M.F.-S. was supported by a senior fellowship from the Medical Research Council (MRC) and S.P. was supported by a DT fellowship from Biotechnology and Biological Sciences Research Council (BBSRC).

## REFERENCES

1. Baker, D.J., Chen, J. and van Deursen, J.M.A. (2005) The mitotic checkpoint in cancer and aging: what have mice taught us? *Curr. Opin. Cell Biol.*, **17**, 583–589.
2. Sullivan, M. and Morgan, D.O. (2007) Finishing mitosis, one step at a time. *Nat. Rev. Mol. Cell Biol.*, **8**, 894–903.
3. Choi, E., Choe, H., Min, J., Choi, J.Y., Kim, J. and Lee, H. (2009) BubR1 acetylation at prometaphase is required for modulating APC/C activity and timing of mitosis. *EMBO J.*, **28**, 2077–2089.
4. Kulukian, A., Han, J.S. and Cleveland, D.W. (2009) Unattached kinetochores catalyze production of an anaphase inhibitor that requires a Mad2 template to prime Cdc20 for BubR1 binding. *Dev. Cell*, **16**, 105–117.
5. Malureanu, L.A., Jeganathan, K.B., Hamada, M., Wasilewski, L., Davenport, J. and van Deursen, J.M. (2009) BubR1 N terminus acts as a soluble inhibitor of cyclin B degradation by APC/C(Cdc20) in interphase. *Dev. Cell*, **16**, 118–131.
6. Peters, J.M. (2006) The anaphase promoting complex/cyclosome: a machine designed to destroy. *Nat. Rev. Mol. Cell Biol.*, **7**, 644–656.
7. Hanks, S., Coleman, K., Reid, S., Plaja, A., Firth, H., Fitzpatrick, D., Kidd, A., Méhes, K., Nash, R., Robin, N. *et al.* (2004) Constitutional aneuploidy and cancer predisposition caused by biallelic mutations in BUB1B. *Nat. Genet.*, **36**, 1159–1161.
8. Matsuura, S., Matsumoto, Y., Morishima, K.-I., Izumi, H., Matsumoto, H., Ito, E., Tsutsui, K., Kobayashi, J., Tauchi, H., Kajiwara, Y. *et al.* (2006) Monoallelic BUB1B mutations and defective mitotic-spindle checkpoint in seven families with premature chromatid separation (PCS) syndrome. *Am. J. Med. Genet. A*, **140**, 358–367.
9. Ganner, A., Lienkamp, S., Schäfer, T., Romaker, D., Wegierski, T., Park, T.J., Spreitzer, S., Simons, M., Gloy, J., Kim, E. *et al.* (2009) Regulation of ciliary polarity by the APC/C. *Proc. Natl Acad. Sci. USA*, **106**, 17799–17804.
10. Gerdes, J.M., Davis, E.E. and Katsanis, N. (2009) The vertebrate primary cilium in development, homeostasis, and disease. *Cell*, **137**, 32–45.
11. Goetz, S.C. and Anderson, K.V. (2010) The primary cilium: a signalling centre during vertebrate development. *Nat. Rev. Genet.*, **11**, 331–344.
12. Nigg, E.A. and Raff, J.W. (2009) Centrioles, centrosomes, and cilia in health and disease. *Cell*, **139**, 663–678.
13. Matsuura, S., Ito, E., Tauchi, H., Komatsu, K., Ikeuchi, T. and Kajii, T. (2000) Chromosomal instability syndrome of total premature chromatid separation with mosaic variegated aneuploidy is defective in mitotic-spindle checkpoint. *Am. J. Hum. Genet.*, **67**, 483–486.
14. Izumi, H., Matsumoto, Y., Ikeuchi, T., Saya, H., Kajii, T. and Matsuura, S. (2009) BubR1 localizes to centrosomes and suppresses centrosome amplification via regulating Plk1 activity in interphase cells. *Oncogene*, **28**, 2806–2820.
15. Simons, M., Gloy, J., Ganner, A., Bullerkotte, A., Bashkurov, M., Krönig, C., Schermer, B., Benzing, T., Cabello, O.A., Jenny, A. *et al.* (2005) Inversin, the gene product mutated in nephronophthisis type II, functions as a molecular switch between Wnt signaling pathways. *Nat. Genet.*, **37**, 537–543.
16. Park, T.J., Mitchell, B.J., Abitua, P.B., Kintner, C. and Wallingford, J.B. (2008) Dishevelled controls apical docking and planar polarization of basal bodies in ciliated epithelial cells. *Nat. Genet.*, **40**, 871–879.

17. Listovsky, T., Oren, Y.S., Yudkovsky, Y., Mahbubani, H.M., Weiss, A.M., Lebendiker, M. and Brandeis, M. (2004) Mammalian Cdh1/Fzr mediates its own degradation. *EMBO J.*, **23**, 1619–1626.
18. Nilsson, J., Yekezare, M., Minshull, J. and Pines, J. (2008) The APC/C maintains the spindle assembly checkpoint by targeting Cdc20 for destruction. *Nat. Cell Biol.*, **10**, 1411–1420.
19. Furutani-Seiki, M. and Wittbrodt, J. (2004) Medaka and zebrafish, an evolutionary twin study. *Mech. Dev.*, **121**, 629–637.
20. Yu, H. (2007) Cdc20: a WD40 activator for a cell cycle degradation machine. *Mol. Cell*, **27**, 3–16.
21. Shirayama, M., Toth, A., Galova, M. and Nasmyth, K. (1999) APC(Cdc20) promotes exit from mitosis by destroying the anaphase inhibitor Pds1 and cyclin Clb5. *Nature*, **402**, 203–207.
22. Wirth, K.G., Ricci, R., Gimenez-Abian, J.F., Taghybeeglu, S., Kudo, N.R., Jochum, W., Vasseur-Cognet, M. and Nasmyth, K. (2004) Loss of the anaphase-promoting complex in quiescent cells causes unscheduled hepatocyte proliferation. *Genes Dev.*, **18**, 88–98.
23. Konishi, Y., Stegmuller, J., Matsuda, T., Bonni, S. and Bonni, A. (2004) Cdh1-APC controls axonal growth and patterning in the mammalian brain. *Science*, **303**, 1026–1030.
24. Jaspersen, S.L., Charles, J.F. and Morgan, D.O. (1999) Inhibitory phosphorylation of the APC regulator Hct1 is controlled by the kinase Cdc28 and the phosphatase Cdc14. *Curr. Biol.*, **9**, 227–236.
25. Clement, A., Solnica-Krezel, L. and Gould, K.L. (2011) The Cdc14B phosphatase contributes to ciliogenesis in zebrafish. *Development*, **138**, 291–302.
26. Wasch, R., Robbins, J.A. and Cross, F.R. (2010) The emerging role of APC/CCdh1 in controlling differentiation, genomic stability and tumor suppression. *Oncogene*, **29**, 1–10.
27. Tucker, R.W., Pardee, A.B. and Fujiwara, K. (1979) Centriole ciliation is related to quiescence and DNA synthesis in 3T3 cells. *Cell*, **17**, 527–535.
28. Rieder, C.L., Jensen, C.G. and Jensen, L.C. (1979) The resorption of primary cilia during mitosis in a vertebrate (PtK1) cell line. *J. Ultrastruct. Res.*, **68**, 173–185.
29. Qin, H., Wang, Z., Diener, D. and Rosenbaum, J. (2007) Intraflagellar transport protein 27 is a small G protein involved in cell-cycle control. *Curr. Biol.*, **17**, 193–202.
30. Spektor, A., Tsang, W.Y., Khoo, D. and Dynlacht, B.D. (2007) Cep97 and CP110 suppress a cilia assembly program. *Cell*, **130**, 678–690.
31. Aboualaiwi, W.A., Ratnam, S., Booth, R.L., Shah, J.V. and Nauli, S.M. (2011) Endothelial cells from humans and mice with polycystic kidney disease are characterized by polyploidy and chromosome segregation defects through survivin down-regulation. *Hum. Mol. Genet.*, **20**, 354–367.
32. Kishida, S., Hamao, K., Inoue, M., Hasegawa, M., Matsuura, Y., Mikoshiba, K., Fukuda, M. and Kikuchi, A. (2007) Dvl regulates endo- and exocytotic processes through binding to synaptotagmin. *Genes Cells*, **12**, 49–61.
33. Porazinski, SR, Wang, H. and Furutani-Seiki, M. (2011) Essential techniques for introducing medaka to a zebrafish laboratory—toward combined use of medaka and zebrafish for further genetic dissection of the function of the vertebrate genome. *'Vertebrate embryogenesis, Methods and Protocols' in the series Methods in Molecular Biology*. Humana Press (in press).
34. Borovina, A., Superina, S., Voskas, D. and Ciruna, B. (2010) Vangl2 directs the posterior tilting and asymmetric localization of motile primary cilia. *Nat. Cell Biol.*, **12**, 407–412.